Cl_2/O_2- and Cl_2/N_2-based Inductively Coupled Plasma Etching of Photonic Crystals in InP: Sidewall Passivation

R. van der Heijden[a,b], C.F. Carlström[a,b], E. van der Drift[c], R.W. van der Heijden[a,b], R. Nötzel[a], R. van Veldhoven[a], F. Karouta[a], H.W.M. Salemink[a,b,c], A. Talneau[d]

[a]COBRA Inter-University Research Institute, Eindhoven University of Technology, PO Box 513, NL 5600 MB Eindhoven, The Netherlands

[b]Center for NanoMaterials, Eindhoven University of Technology, PO Box 513, NL 5600 MB Eindhoven, The Netherlands

[c]Kavli Institute of Nanoscience, Delft University of Technology, P.O. Box 5053, 2600 GB Delft, The Netherlands

[d]CNRS/Laboratoire de Photonique et de Nanostructures, Route de Nozay, F-91460 Marcoussis, France

We have fabricated two-dimensional photonic crystals in InP-based materials with Cl_2-based inductively coupled plasma etching. To obtain vertical sidewalls, we employ sidewall passivation through addition of N_2 or O_2 to the plasma. With the Cl_2/O_2-process we are able to etch 3.2 μm deep holes that have nearly cylindrical shape in the upper 2 μm. The first optical results illustrate the feasibility of our approach, showing over 30 dB transmission reduction in the ΓK-stopband.

I. Introduction

InP based two-dimensional (2D) photonic crystals could be present in many of the future optical devices involving the telecommunication wavelength of 1550 nm. For guided optics applications on semiconductor materials the etched holes are placed on a triangular lattice with a pitch of a~400 nm, have diameter of d~250 nm and are etched through an InP/InGaAsP/InP planar waveguide structure. To minimize optical loss, the holes should be ~2.5 μm deep and exhibit smooth and vertical sidewalls (1). Excellent results have been achieved with chemically assisted ion beam etching (CAIBE) (2), (3) and electron cyclotron resonance reactive ion etching (ECR-RIE) (4) using Ar/Cl_2-chemistry. A versatile technique for large-scale fabrication is inductively coupled plasma (ICP) etching. This technique provides high etch rate due to high current density and allows independent control of the ion energy. Excellent results on deep-hole etching have been obtained with ICP using $SiCl_4$-chemistry (5). We have previously reported on ICP etching of hole-type photonic crystals using Cl_2 chemistry (6), (7). Reasonably deep holes (2.3 μm) could be etched, but with sloped sidewalls (87°) and significant undercut in the top region. Since the limited hole depth requires the guiding core layer to be in close vicinity to the top surface these undercut regions may cause significant optical loss (8). To improve the undercut and the sidewall verticality simultaneously, modification of the Cl_2-chemistry should be investigated. It has been shown that for Si dry etching, sidewall passivation is a mandatory tool for fabrication of high aspect ratio features (9). Si-based photonic crystal pillars have been etched with SF_6 as the chemical component and O_2 for passivation (10). Low aspect ratio (<1) features with vertical sidewalls have been etched with RIE in InP based materials with both Cl_2/O_2- (11) and Cl_2/N_2-mixtures (12). In the present paper, we report Cl_2-based ICP etching of high aspect ratio (>10) photonic crystal holes in InP-based materials with addition of N_2 or O_2 for sidewall passivation.

II. Experimental

Experiments were performed on (100) n-type Sn-doped InP substrates with a size of approximately 8x8 mm^2. The photonic crystal pattern is defined into a layer of PMMA or ZEP520A (positive e-beam resist) with e-beam lithography. This pattern is then transferred into a 400 nm thick, PECVD deposited SiN_x-masking layer with a CHF_3-based RIE process. After the final ICP etch step the samples were cleaved and the cross-section was inspected with a scanning electron microscope (SEM). ICP etch experiments were carried out in an Alcatel MET system (Cl_2/N_2) and in an Oxford Plasmalab 100 system (Cl_2/O_2). As the main etch-product, $InCl_3$, is not enough volatile at room temperature, all etching was performed at elevated temperature (180-250 °C) to ensure chemical etching by Cl (13). Sample temperature control in ICP etching can be difficult due to significant heating by the ion bombardment (14). The samples were glued with heat conducting paste onto a 4 in. silicon (Plasmalab) or stainless steel (MET) carrier wafer. In the MET a He-backflow provided thermal contact between the wafer and the substrate holder. To limit sample heating during etching in the Plasmalab, sequenced processing was used with etch runs of 30 s. The temperature of the substrate holder was measured

0-7803-8891-7/05/$20.00 ©2005 IEEE

with a thermocouple (Plasmalab) or a Luxtron fluoroptic probe (MET). The ion energy was controlled by the DC-bias voltage, which is induced by capacitive coupling of additional rf-power to the plasma. Various structures were etched for SEM-evaluation of the etching process, including photonic crystal holes with diameters ranging from 160 nm to 1000 nm and 10 μm wide trenches. For optical characterization, a lithographically tuned (15) photonic crystal with a designed air filling factor $f = 0.33$ was etched with the Cl_2/O_2-process through a MOCVD grown planar waveguide sample for vertical optical confinement. The grown structure consists of a 500 nm thick InGaAsP ($\lambda = 1.25$ μm) core and a 500 nm thick InP upper cladding. Access ridge waveguides were patterned in the same e-beam step as the photonic crystal sections on this sample and also etched in the same ICP-etching step. Transmission measurements were performed with a fiber-to-fiber end-fire set-up with a wavelength tuning range of 1410-1585 nm (16).

III. Results

A. Cl_2/N_2 results

To investigate the passivation capabilities of N_2, experiments were performed in the MET system for both

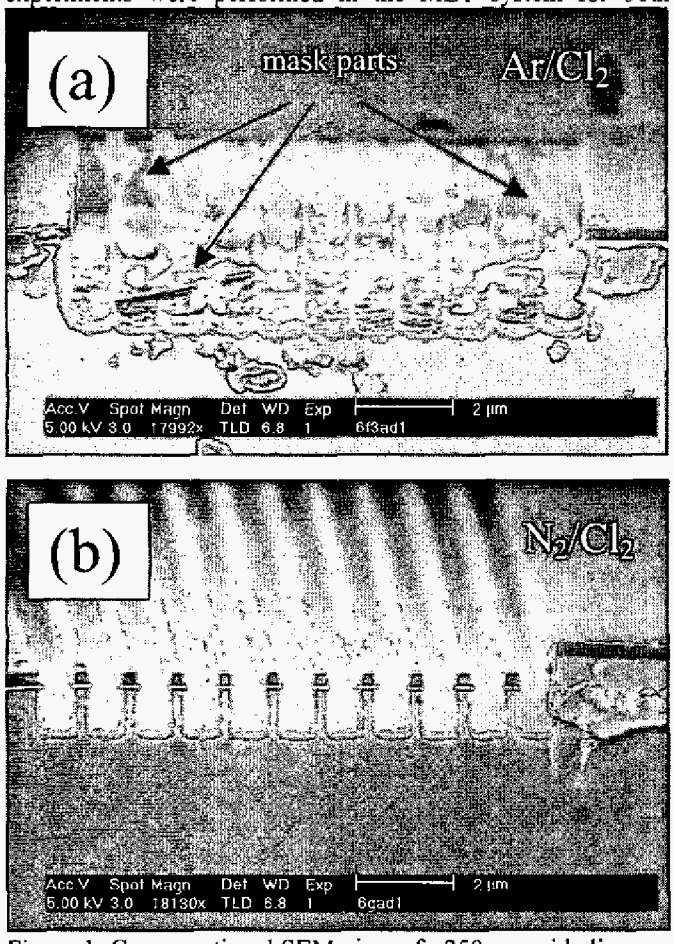

Figure 1: Cross-sectional SEM view of ~250 nm wide lines on a 1000 nm pitch etched with (a) Ar/Cl_2 and (b) N_2/Cl_2 with otherwise identical process parameters.

Ar/Cl_2- and N_2/Cl_2-chemistry. The reactor pressure was set to 1.0 Pa with an Ar or N_2-flow of 75 sccm and a Cl_2-flow of 25 sccm. The substrate temperature was set to 220 °C to ensure spontaneous etching in the Ar/Cl_2 case. The ICP-source power was set to 1000 W and the DC-bias was kept at –100 V. SEM images of ~250 nm wide lines on a 1000 nm pitch after 2 minutes of etching are shown in figure 1. In the Ar/Cl_2 process significant lateral etching occurs as can be concluded from the undercut at the sides of the structured field in figure 1(a). This undercut is so large, that the lines are completely etched away, leaving residual SiN_x-mask parts. Figure 1(b) shows the result of the N_2/Cl_2-process. In this case no undercut is observed. The sidewalls of the features are vertical, except for a slight bowing, which can be attributed to ion-induced effects (17). Evidently, sidewall passivation plays an important role here. We have shown before that a N_2:Cl_2-ratio of 3:1 is required for proper passivation with these process parameters, which implies that Cl_2 is the minority species in the plasma. This fundamental limitation of reactive chlorine supply (12) will lower the InP etch rate significantly compared to the Cl_2 only case, as the etching process in this regime is neutral limited (7). Furthermore, the InP etch rate is decreased by passivation of the feature bottom surface (12). These effects limit the InP:SiN_x selectivity, as the etching mechanism of the SiN_x mask is mainly physical. Although photonic crystal holes with vertical sidewalls were achieved after some process optimization, the etch depth was limited to 1 μm (7). To overcome this limitation, a gas with stronger passivation capabilities, such as O_2, should be used. In this way, the supply of reactive chlorine to the InP-surface can be left mostly unaffected.

B. Cl_2/O_2 results

Experiments with Cl_2/O_2 chemistry were performed in the Plasmalab system. The reactor pressure was set to 0.26 Pa with a Cl_2-flow of 7 sccm and an O_2-flow of 1.8 sccm. The substrate temperature was set to 250 °C to ensure spontaneous etching in the Cl_2-only case. The ICP-source power was set to 500 W and the DC-bias was kept at –500 V. SEM images of ~200 nm diameter holes on a 800 nm pitch after 1 minute of etching are shown in figure 2. For the Cl_2-only process (figure 2(a)) significant lateral etching occurs in the top part of the hole. The addition of only 1.8 sccm of O_2 is sufficient to prevent this lateral etching, yielding photonic crystal holes with vertical sidewalls. This sidewall passivation leads to larger hole depth as the chlorine radicals that were consumed for lateral etching are now consumed at the bottom of the hole. Balancing the Cl_2- and O_2-flow is crucial for the final etching result, as is visible in figure 3. In this figure the feature-size dependent etch-depth is shown for a Cl_2-flow of 14 sccm and O_2-flow of 1.8, 2.6 and 3.6 sccm, with otherwise the same process parameters as stated above. For the process with 1.8 sccm O_2, the etch depth of the 10 μm wide trench was more than 7 μm. The etch depth of the ~200 nm diameter holes is ~3.2 μm, which implies a RIE-lag (18) of more than a factor of 2 for these holes. In the upper 2 μm the shape of the holes is

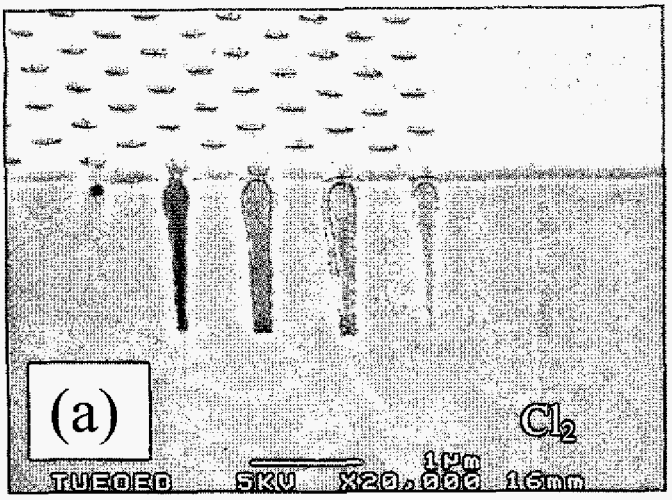

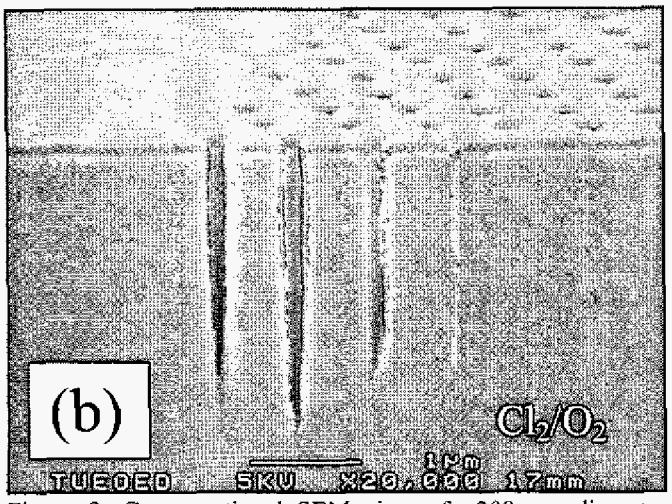

Figure 2: Cross-sectional SEM view of ~200 nm diameter holes on an 800 nm pitch etched with (a) Cl_2-only and (b) Cl_2/O_2 with otherwise identical process parameters. Structures are cleaved under a small angle (~3°) with the ΓM-direction.

nearly cylindrical. Increasing the flow to 2.6 sccm does not significantly change the etch depth for all feature sizes. Further increase to 3.6 sccm however, causes a decrease of the trench etch depth with a factor of 2, which is attributed to improved bottom passivation. Apparently, a certain threshold oxygen abundance is required for the bottom passivation to be strong enough to partly withstand the ion bombardment and inhibit etching. In high aspect ratio features the radical density is depleted (18) and not enough oxygen is available at the bottom to inhibit etching. Therefore the depth of the small holes does not change significantly in this flow regime. Processes yielding the highest hole-quality produce ridges with rough and undercut sidewalls. For etching of access ridge waveguides and photonic crystal fields in a single step, a compromise between ridge and hole quality should be found. A sample was prepared for preliminary optical experiments using the same process as for the result in figure 2(b).

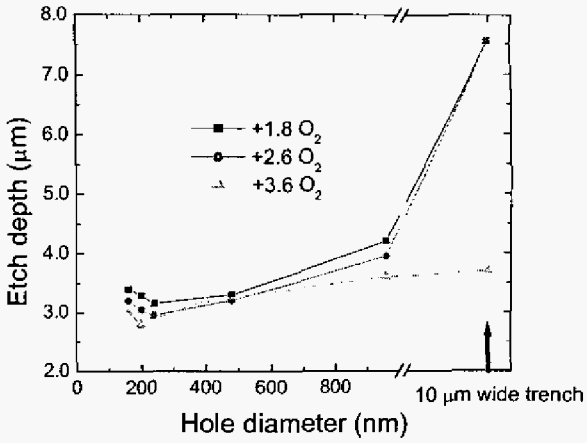

Figure 3: Feature-size dependent etch depth for a Cl_2-flow of 14 sccm and O_2-flows of 1.8, 2.6 and 3.6 sccm after 1 minute of etching. The etch depth of a 10 μm wide trench is included for comparison.

C. Optical results

For optical characterization, a sample was fabricated with 2.5 μm wide ridge waveguides intersected by a photonic crystal field. A side view of this configuration is shown in figure 4. Unfortunately, the ridge-sidewalls are rough and notched at the level of the waveguide core layer, leading to high propagation losses. Similar ridge profiles were observed on an InP control sample, which was etched in the same run as the planar waveguide sample. This profile is therefore related to the etching process itself and not to the material composition. SEM inspection of the control sample cross-section showed that the photonic crystal holes had similar profiles as the ones in figure 2(b). The photonic crystal fields consist of a triangular lattice of holes with 9 periods in the ΓK-direction, coinciding with the propagation direction of the ridge waveguides. To scan the stopgap on a normalized frequency scale, lithographic tuning was employed (15). The filling fraction of the fabricated photonic crystals was measured with the SEM from top. It turns out that the fabricated f was somewhat smaller than designed, ranging from $f = 0.31$ for a = 307 nm to $f = 0.25$ for a = 559 nm. The transmission spectrum of the photonic crystal is shown in the graph at the bottom of figure 4. As some of the ridges were damaged, not all structures could be measured. The small stitching mismatch that is observed between the overlapping spectra (0.8 % between a = 307 and 336 nm, 1.3 % between a = 509 and 559 nm) can be attributed to effective index dispersion and small filling factor variations (15). The ΓK band edges were calculated with a plane wave expansion method using the measured filling factors.

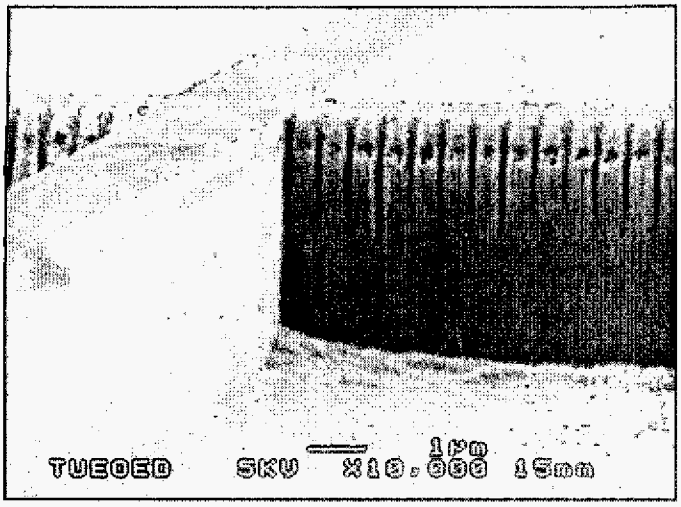

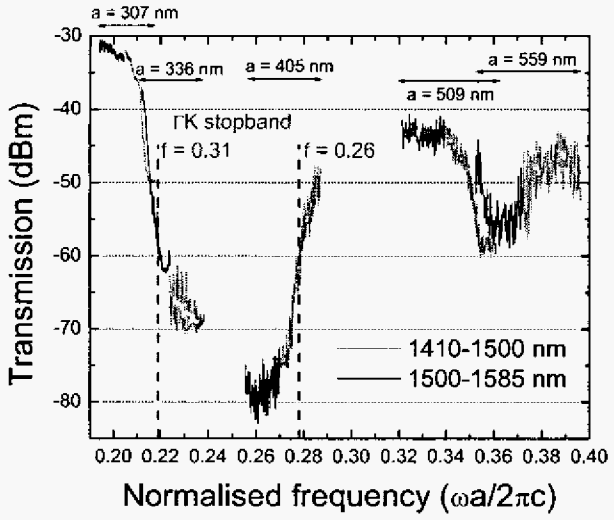

Figure 4: *Top*: side view of a measured structure, consisting of a 2.5 μm ridge waveguide intersected by a photonic crystal field. The outer holes of the field are exposed to the open area. Their shape and depth are therefore not representative for the inner holes. *Bottom*: graph of the measured transmission in the ΓK-direction of the crystal. The lattice constants are denoted in the top of the graph, the used laser source is indicated by the line color. The band edges are calculated for $f = 0.31$ (dielectric band) and $f = 0.26$ (air band). The effective index used was 3.25.

We find good agreement between the calculated band edges and the measured transmission spectrum. Note the >30 dB transmission decrease and increase for single measured crystals at the band edges. In the air band, the electric field is localized inside the air-holes leading to larger losses (19) and an in our case ~10 dB lower transmission level compared to the dielectric band. Starting from normalized frequency of 0.35 a second transmission dip is visible in the measured spectrum, which is also observed in 2D FDTD calculations (5).

Acknowledgements

The authors would like to thank E.J. Geluk and P. Nouwens for technical assistance. Part of this research is supported by NanoNed, a technology programme of the Dutch ministry of Economic Affairs.

References

1. R. Ferrini, R. Houdré, H. Benisty, M. Qiu, J. Moosburger, J. Opt. Soc. Am. B **20**, 469 (2003).
2. M.V. Kotlyar, T. Karle, M.D. Settle, L. O'Faolain, T.F. Krauss, Appl. Phys. Lett. **84**, 3588 (2004).
3. M. Mulot, S. Anand, R. Ferrini, B. Wild, R. Houdré, J. Moosburger, A. Forchel, J. Vac. Sci. Technol. B **22**, 707 (2004).
4. T.D. Happ, A. Markard, M. Kamp, A. Forchel, S. Anand, J.L. Gentner, N. Bouadma,. J. Vac. Sci. Technol. B **19**, 2775 (2001).
5. F. Pommereau, L. Legouezigou, S. Hubert, S. Sainson, J.P. Chandouineau, S. Fabre, G.H. Duan, B. Lombardet, R. Ferrini, R. Houdre. J. Appl. Phys. **95**, 2242 (2004).
6. R. van der Heijden, M.S.P. Andriesse, C.F. Carlström, E. van der Drift, E.J. Geluk, R.W. van der Heijden, F. Karouta, P. Nouwens, Y.S. Oei, T. de Vries, H.W.M. Salemink, Proc. SPIE 5450, 523 (2004).
7. R. van der Heijden, C.F. Carlström, M.S.P. Andriesse, E. van der Drift, E.J. Geluk, R.W van der Heijden, F. Karouta, P. Nouwens, Y.S. Oei, T. de Vries, H.W.M. Salemink, Proceedings Symposium IEEE/LEOS Benelux Chapter, Ghent, 287 (2004).
8. R. Ferrini, A. Berrier, L. A. Dunbar, R. Houdré, M. Mulot, S. Anand, S. de Rossi, A. Talneau, Appl. Phys. Lett. **85**, 3998 (2004).
9. M.A. Blauw, E. van der Drift, G. Marcos, A. Rhallabi, J. Appl. Phys. **94**, 6311 (2003).
10. T. Zijlstra, E. van der Drift, M.J.A. de Dood, E. Snoeks, A.Polman, J. Vac. Sci. Technol. B **17**, 2734 (1999).
11. L.A. Coldren, and J.A. Rentschler, J. Vac. Sci. Technol. **19**, 225 (1981).
12. S. Miyakuni, R. Hattori, K. Sato, H. Takano, O. Ishihara, J. Appl. Phys. **78**, 5734 (1995).
13. S.C. McNevin, J. Vac. Sci. Technol. B **4**, 1216 (1986).
14. E. Sabin, J. Vac. Sci. Technol. B **16**, 1841 (1998).
15. D. Labilloy, H. Benisty, C. Weisbuch, C.J.M. Smith, T.F. Krauss, R. Houdré, U. Oesterle, Phys. Rev. B **59**, 1649 (1999).
16. A. Talneau, L. Le Gouezigou and N. Bouadma, Opt. Lett. **26**, 1259 (2001).
17. G. Marcos, and A. Rhallabi, J. Vac. Sci. Technol. A **21**, 87 (2002).
18. R.A. Gottscho, C.W. Jurgensen, D.J. Vitkavage, J. Vac. Sci. Technol. B **10**, 2133-2147 (1992).
19. Ph. Lalanne, H. Benisty, J. Appl. Phys. **89**, 1512 (2001).